Geomechanics and Engineering, *Vol. 37, No. 6 (2024) 615-627*
https://doi.org/10.12989/gae.2024.37.6.615

A novel dual stress/strain-controlled direct simple shear apparatus to study shear strength and shear creep of clay

Chen Ge[1a], Zhu Jungao*[1], Wang Tao**[2], Li Jian[3b], Lou Qixun[3c] and Li Tao[3d]

[1]*Key Laboratory of Ministry of Education for Geomechanics and Embankment Engineering, Hohai University, Nanjing 210098, China*
[2]*School of Earth Sciences and Engineering, Nanjing University, Nanjing 210023, P.R. China*
[3]*Chengdu Engineering Corporation Limited, Chengdu 610072, China*

(*Received April 1, 2024, Revised May 23, 2024, Accepted June 4, 2024*)

Abstract. Direct simple shear test is an effective method to measure strength and deformation properties of soil. However, existing direct simple shear apparatus have some shortcomings. The paper has developed a novel dual stress/strain-controlled direct simple shear apparatus. The novel apparatus has the following advantages: A rectangular specimen is used that effectively avoid common issues associated with conventional cylindrical specimens, such as specimen tilting. The utilization of deformation control rods ensures a uniform shear deformation of the specimen. Vertically integrated force transmission structure is improved that avoids issues arising from changes in pivot points due to lever tilting. Incorporating this novel direct simple shear apparatus, shear strength and shear creep tests of clay were performed. Shear strength parameters and shear creep behaviors are analyzed. The results of these experiments show that the novel apparatus can measure accurately the shear rheological properties of soil. This study provides strong guidance for studying the mechanical properties of soil in engineering practice.

Keywords: creep test; direct simple shear apparatus; shear strength test; steel laminations; stress/strain control; uniform shearing

1. Introduction

The study of soil stress-strain behavior commonly relies on laboratory testing methods such as triaxial, direct shear, and direct simple shear tests. Among these, the direct simple shear test stands out for its ability to approximate the pure shear state of soil, rendering it valuable across a spectrum of practical engineering applications including seismic analysis, offshore foundation assessment, and slope stability analysis (Vucetic and Lacasse 1982, Vieira *et al*. 2015, Zhang *et al*. 2016, Rasool and Aziz 2019, Dang *et al*. 2022, Muhammad *et al*. 2023, Tao *et al*. 2023). Compared to the direct shear apparatus, the direct simple shear apparatus offers advantages such as a more uniform internal stress distribution within the specimen, a non-fixed failure surface, and the capability to measure shear strain in the soil (Jurko *et al*. 2008). Furthermore, in contrast to the triaxial apparatus, the preparation of specimens for the direct simple shear test is simpler, allows for rapid consolidation, and yields strength properties more akin to practical engineering scenarios (Mayne 1985, Airey and Wood 1987, Cappellaro *et al*. 2021, Wai *et al*. 2022). Consequently, the direct simple shear test has garnered significant attention and enjoys widespread adoption for determining the mechanical properties of soils.

The inception of the direct simple shear test can be traced back to the development of the earliest ring shear apparatus by the Swedish Geotechnical Institute in 1936 (Kjellman 1951, Bjerrum and Landva 1966, Li *et al*. 2017, Nong *et al*. 2021). This apparatus utilized lateral rubber membranes to confine the specimen, encasing it within multiple aluminum rings to maintain a constant cross-sectional area. Subsequent iterations of similar apparatuses were pioneered by institutions such as Cambridge University and the Norwegian Geotechnical Institute, each employing distinctive methodologies for specimen confinement and shear force application (Roscoe 1953, Budhu 1984, 1987, 1988, Doroudian and Vucetic 1995, Vucetic *et al*. 1998). Norwegian Geotechnical Institute' apparatus uses cylindrical specimens and employing rubber membranes reinforced with steel wires for lateral confinement. The apparatus developed by Cambridge University uses rigid boundaries to constrain the soil, and the soil is a cuboidal sample. There are two hinged side plates at both ends of the pressure chamber that can rotate, and when rotated, they are parallel to each other, resulting in uniform shear strain of the soil sample.

In the ensuing years, numerous advancements were made to enhance the performance and functionality of these shear apparatuses. Notable developments include Geonor's

*Corresponding author, Professor
E-mail: caw22731@163.com
**Corresponding author, Ph.D.
E-mail: tao_wang@nju.edu.cn
[a]Ph.D.
[b]Ph.D.
[c]Ph.D.
[d]Ph.D.

ISSN: 2005-307X (Print), 2092-6219 (Online)

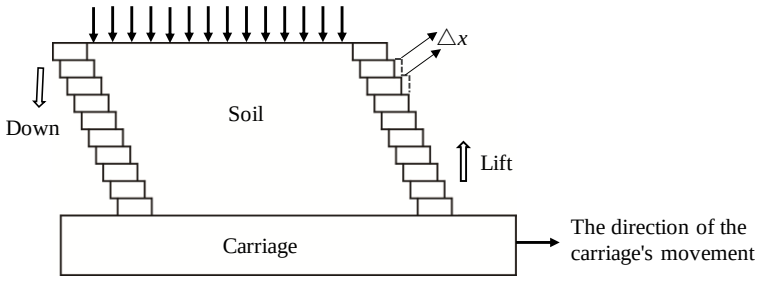

Fig. 1 Schematic diagram of shear deformation in normal direct simple shear apparatus

DSS and the cylindrical constant stress simple shear apparatus (CSSA) described by Airey and Wood, both of which featured cylindrical specimens wrapped in rubber membranes reinforced with spiral coils (DeGroot *et al*. 1996, Airey and Wood 1987). And, fully automated iterations of the NGI-type DSS and CSD apparatuses were introduced, boasting improved automation capabilities and specimen confinement techniques (Lashkari *et al*. 2020, Anderson and Riemer 1995, Chu *et al*. 2012, Reid and Fourie 2019). Additionally, hollow cylinder torsional shear devices have been used that the device can perform tests with both stress and strain controls (Khayat *et al*. 2014, Khayat 2018). It can measure the anisotropy of soil.

Moreover, commercial entities such as Geotechnical Consulting and Testing Systems (GCTS) in the United States and the British GDS company have contributed to the advancement of shear apparatus technology with products like the CSS apparatus and EMDCSS/VDDCSS, respectively (Hubler *et al*. 2017, Kwan and Shun 2018, Reardon *et al*. 2022, Li *et al*. 2017, Zhang *et al*. 2019, Jin *et al*. 2022). These innovations typically focus on automation, material selection, and specimen dimensions to enhance test efficiency and accuracy.

However, despite these advancements, certain challenges persist in existing direct simple shear apparatuses, particularly regarding structural aspects such as the pressure chamber, cylindrical specimen design, and the use of rubber membranes. These challenges, including non-uniform stress distribution at specimen boundaries and issues related to specimen stability, necessitate further improvements in shear apparatus design.

In response to these challenges, this paper presents a novel stress/strain-controlled direct simple shear apparatus that addresses some of the limitations of current mainstream shear apparatuses. The apparatus has undergone preliminary experiments, including shear strength tests for two types of soils and shear creep tests under different stress levels, demonstrating its potential utility in soil mechanics research.

2. Design and development of a novel stress/strain-controlled direct simple shear apparatus

2.1 Design requirement

The development of a novel stress/strain-controlled direct simple shear apparatus needs to meet several key design requirements:

(1) The direct simple shear apparatus is designed to incorporate a specimen chamber without a rubber membrane around the specimen. It facilitates specimen preparation. Meanwhile, the specimen chamber can securely hold the steel laminations to prevent soil particles from being squeezed between the layers of steel laminations. It is necessary that this design does not affect the shearing process.

(2) The uppermost steel lamination remains horizontally fixed, while the lowest steel lamination is moved. A notable issue arises during shearing, where one side of the steel laminations tends to lift, resulting in a non-uniform distribution of shear stress (see Fig. 1). Reducing or eliminating the tendency for specimen tipping and rotation during shearing is essential to enhance accuracy of test result.

(3) It is required to maintain an equal shear displacement difference between each pair of adjacent steel laminations (as depicted in Fig. 1), thereby achieving uniform shear deformation of the specimen.

(4) To achieve a more uniform distribution of shear stress, it is necessary to ensure that the specimen experiences shear force in only one horizontal direction. This requires designing a structure that limits the displacement of steel laminations towards other horizontal directions.

(5) When applying vertical loads using a lever, the vertical deformation of the specimen may cause the lever to rotate within the vertical plane. This, in turn, leads to a change in the position of the lever pivot, making it difficult to accurately transmit vertical loads. Therefore, it is necessary to address the issue of pivot change.

2.2 Structure of the novel stress/strain-controlled direct simple shear apparatus

In order to meet the above-mentioned requirements, a novel stress/strain-controlled direct simple shear apparatus has been developed. This apparatus is shown in Fig. 2. It comprises three key components: the specimen box, measurement system, and loading system. The specimen box is the core structure of the direct simple shear apparatus, which is crucial to ensuring the precision of the experiments. It is a challenging aspect of the apparatus development. The measurement system comprises a series of electronic data acquisition devices for automatically collecting force and displacement data. The loading system consists of both horizontal and vertical loading systems. The apparatus is described in detail as follows.

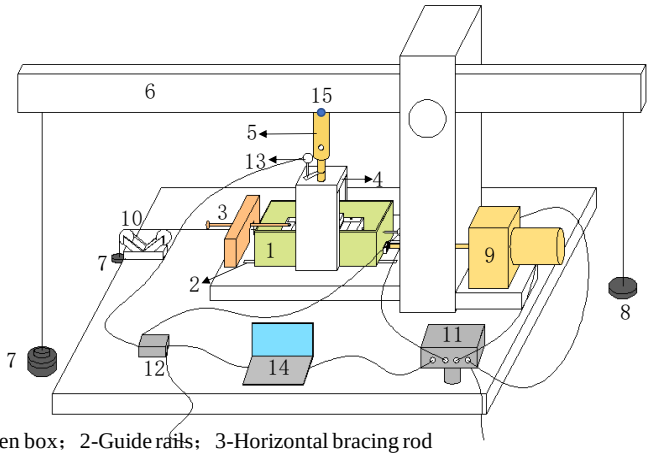

1-Specimen box；2-Guide rails；3-Horizontal bracing rod
Vertical loading system：4-Loading rod support；5-Vertically oriented force transmission structure；
6-Lever； 7-Whights；8-Calibration weights; 15-Pivot point
Horizontal loading system ： 7-Whights；9-Horizontal servo motor；10-Fixed pulley；
11-Digital display controller
Measurement system：12-Hub；13-Displacement sensor；14-Computer

Fig. 2 Novel direct simple-shear apparatus

2.2.1 Specimen box

The specimen box mainly consists of a set of steel laminations, an outer frame for fixing the steel laminations, and a carriage, as illustrated in Fig. 3.

A set of steel laminations consists of 13 rectangular-ambulatory-plane steel laminations. The surfaces of these steel laminations have been polished. The internal dimensions of these steel laminations are 100 mm in length and 40 mm in width, resulting in a length-to-width ratio of 2.5:1 for the specimen. The significantly greater length than width minimizes the tendency of the specimen to tip after shear deformation compared to square or cylindrical specimens. This shape promotes a more uniform distribution of shear stress in the plane.

The top steel lamination, referred to as steel lamination A, is relatively thick (6 mm) to ensure that the bottom of the permeable plate remains within steel lamination A after specimen consolidation. The bottom steel lamination, steel lamination B, has a thickness of 4 mm. The remaining 11 steel laminations, referred to as "thin steel laminations", are each 2 mm thick. During shear testing, steel lamination A remains stationary, and steel lamination B moves with the carriage. The actual shear height of the specimen is depicted in Fig. 4(c).

To ensure uniform shear displacement increments between adjacent layers of thin steel laminations, a pin-controlled deformation control rod is employed. Each layer of the steel laminations is equipped with three waist-shaped apertures in the front of them. Three deformation control rods pass through the three waist-shaped apertures vertically, respectively, as depicted in Fig. 4(a). A through-hole horizontally is set at the front end (define direction of shear stress as the front) of steel lamination A. A pin is inserted into the through-hole and sequentially passes through small holes at the top of the three deformation control rods. The pin allows the deformation control rods to rotate around it (as shown in Fig. 4(b)).

The steel lamination A remains stationary, and steel lamination B is fixed to the carriage. The carriage is pulled results in inclinations of the deformation control rods, causing thin steel laminations displacement (as shown in Fig. 4(c)). To accommodate the required angular deflection of the deformation control rods, it is imperative that the diameter of the waist-shaped apertures must exceed the diameter of the deformation control rods in the shear direction.

The deformation control rods contact with the rearward wall of waist-shaped apertures on steel lamination B, while maintaining clearance at the forward wall. Likewise, they engage with the forward wall of the waist-shaped aperture on thin steel laminations, while preserving clearance at the rearward wall. Furthermore, the deformable control rods exist clearances with both the forward and rearward walls of the waist-shaped aperture on steel lamination A.

Referring to Fig. 4(a), it becomes apparent that when the bottom layer of steel lamination B is pulled, the contact between the rearward wall of the waist-shaped apertures on steel lamination B and the deformation control rod causes the rod to move along with steel lamination B. However, since steel lamination A is fixed, the top of the deformation control rod does not move, and the deformation control rod acts as a rigid body, causing tilting. Simultaneously, the forward wall of the waist-shaped aperture on thin steel laminations comes into contact with the deformation control rod, thereby driving the displacement of the thin steel laminations due to the inclination of the deformation control rod. Given the uniform thickness of the thin steel laminates, identical inclination angles of the deformation control rod lead to consistent increments in displacement among adjacent thin laminates.

Simultaneously, there exists a vertical gap between the bottom end of the deformation control rods and the bottom surface of steel lamination B. The vertical gap ensures that the bottom of the deformation control rods after inclining

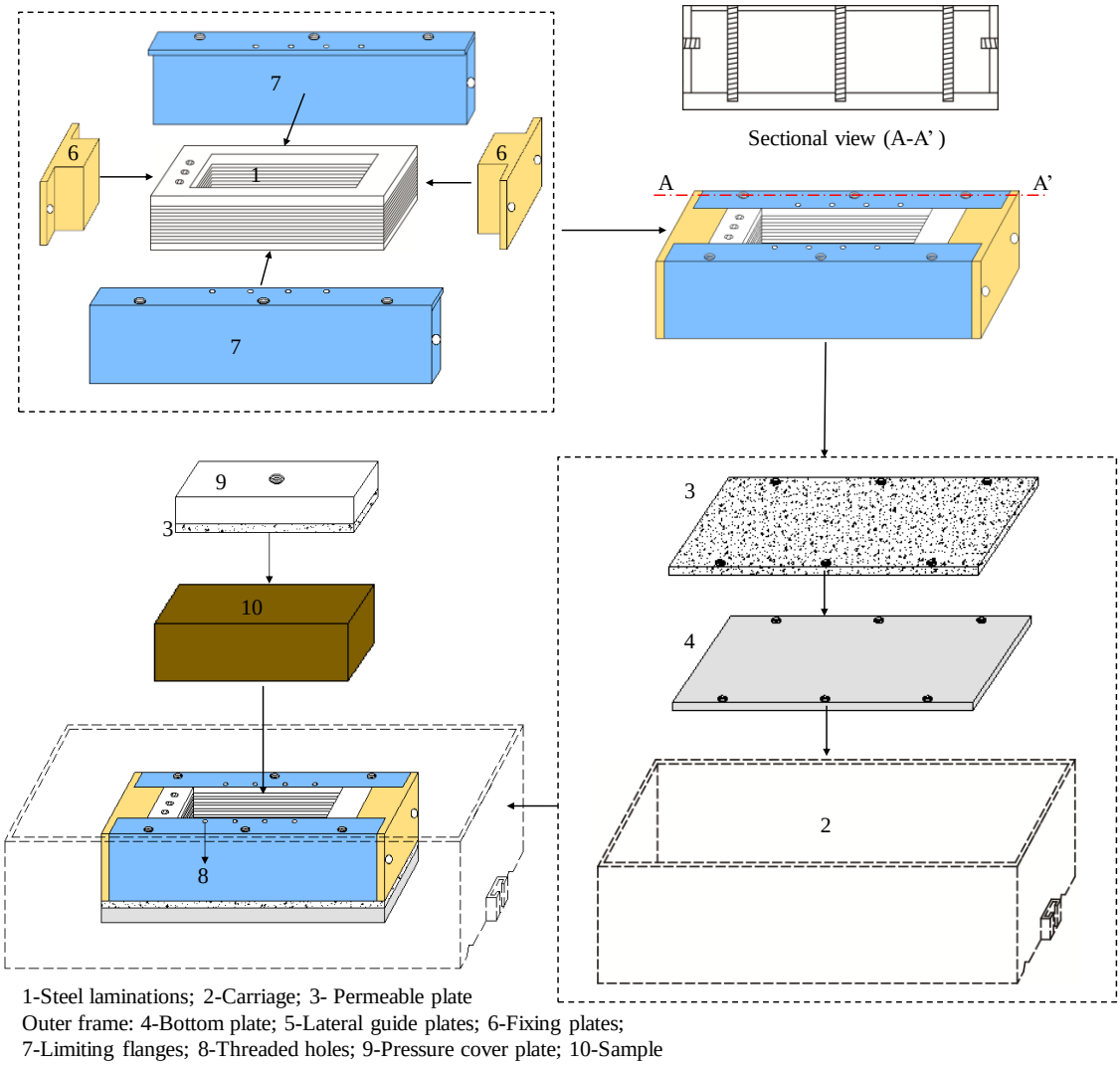

Fig. 3 Assembly diagram of specimen box

does not protrude beyond steel lamination B. The primary function of the deformation control rods is not only to limit the vertical displacement of the steel laminations but, more importantly, to ensure uniform shear displacement among the laminations. It is thereby guaranteed that a uniform distribution of shear strain from top to bottom throughout the test specimen.

The outer frame for fixing the steel laminations is composed of a bottom plate, two lateral guide plates, and two fixing plates. It forms an open-top rectangular cavity, as shown in Fig. 3. The bottom plate is fixed within the carriage. The two lateral guide plates are symmetrically set on the left and right sides of the bottom plate. The two fixing plates are positioned at the front and rear ends of the bottom plate, respectively. A central rectangular cavity where the 13 steel laminations are placed is created. The internal dimensions of the outer frame closely match the plane dimensions of the steel laminations. The outer frame thereby constrains any horizontal sliding of the steel laminations during specimen preparation and consolidation. To prevent friction between the outer frame and the steel laminations during shear testing, there is a 0.1 mm gap between the two lateral guide plates and the steel laminations. The outer frame is designed to be detachable. The two fixing plates in the shear direction are removed during testing, without affecting the lateral sliding of the steel laminations along the shear direction.

The lateral guide plates install limiting flanges in the direction of the central rectangular cavity. Threaded holes are provided on the limiting flanges. Screws are screwed into the threaded holes to press against steel lamination A. The structure ensures that adjacent laminations do not develop gaps during specimen preparation and consolidation, preventing soil from being squeezed between steel laminations. The screws are removed during shear testing to reduce friction between the steel laminations. The lateral guide plates are retained during shear to ensure the steel laminations slide only along the shear direction.

The novel direct simple shear apparatus incorporates a topless rectangular carriage for applying horizontal shear force to the specimen, as depicted in Fig. 3. Meanwhile, because the sample needs to remain saturated after vacuum saturation in the saturation cylinder, the carriage is designed to ensure that the saturated sample remains submerged. The

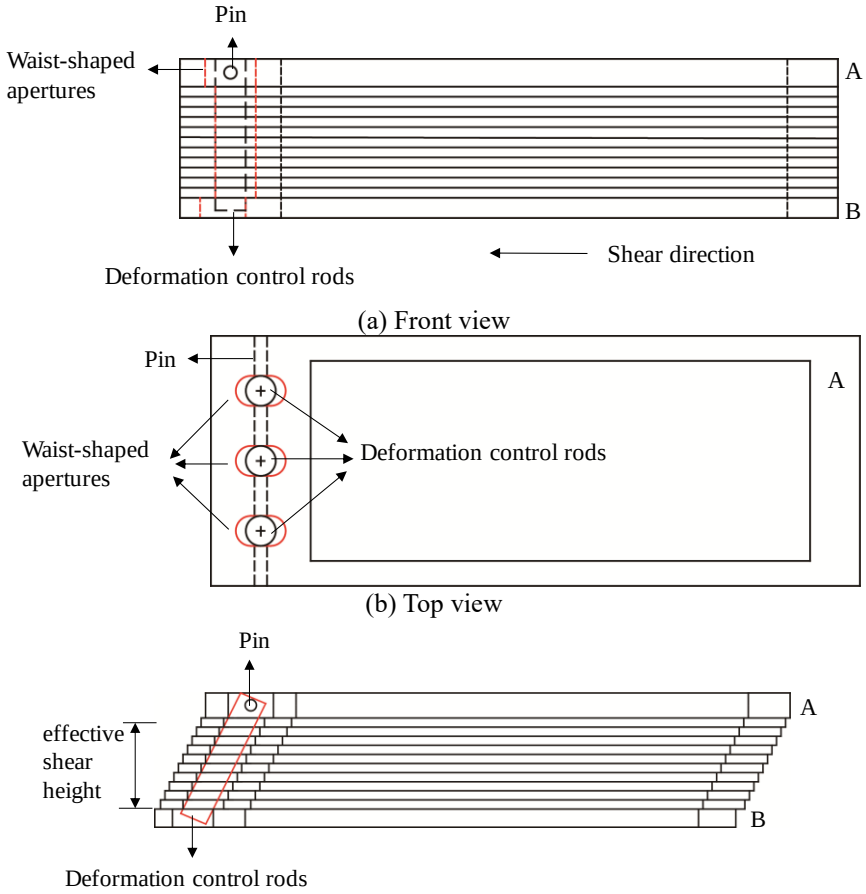

Fig. 4 Schematic diagram of stacked steel laminations

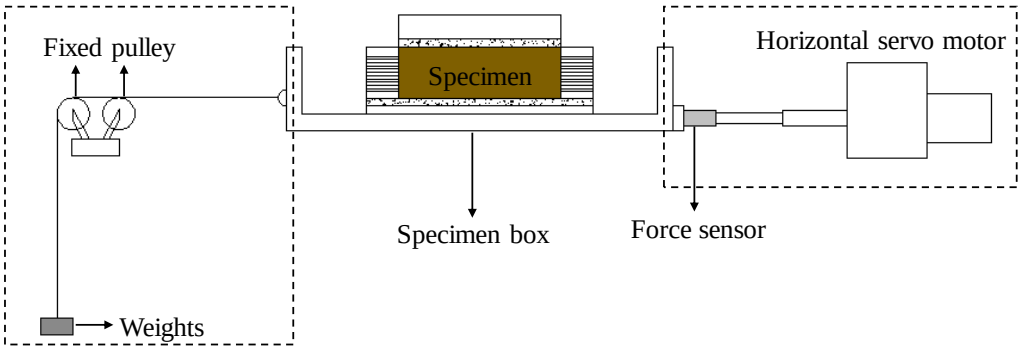

Fig. 5 Horizontal loading system

permeable plate is fixed above the bottom plate of carriage and connected to the frame around steel lamination B for consolidated drained test. Rails are installed underneath the carriage. Small steel balls are placed on the rails. The Vaseline is applied to reduce friction at the bottom of the carriage. The design ensures that the carriage can slide freely in the shear direction during shear.

2.2.2 Measurement and loading systems

The measurement system records displacement or shear force. The loading system applies vertical and horizontal loads to the specimen. Vertical loading is achieved through a lever system. The horizontal loading system comprises two loading modes, as shown in Fig. 5. One mode employs a horizontal servo motor for horizontal loading (strain-controlled loading), and one end of a force sensor is connected to the horizontal servo motor, and the other end is connected to the sample box to measure shear force. The other mode uses weights connected to the carriage via steel wires for horizontal loading (stress-controlled loading). The following text will focus on the lever pivot and the vertical force transmission structure of the vertical loading system (Fig. 6).

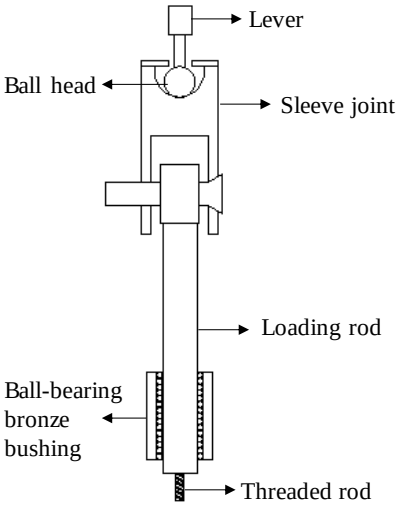

Fig. 6 Diagram of vertical loading system structural cross-section

To ensure that the vertical force is applied at the center of the specimen, the pressure cover plate is fixed to the permeable plate, and the permeable plate is inserted into lamination A by 1-1.5 mm. The lower end of the loading rod is equipped with a threaded rod that can be screwed into the pressure cover plate. The lower section of the loading rod passes through a ball-bearing bronze bushing fixed on the loading rod support. At the upper end of the loading rod, there is a sleeve joint. The loading rod is hinged at the sleeve joint. A spherical groove is incorporated into the sleeve, and a ball head is designed to connect the lever to the sleeve. The sleeve counteracts a portion of the horizontal forces generated by rotation of the lever. This structure solves the problem of vertical load variation caused by lever pivot changes due to vertical soil deformation. The detailed structure is depicted in Fig. 6.

To further eliminate any potential horizontal displacement at the top of the specimen, a horizontal bracing rod (as shown in Fig. 2) is arranged to support the pressure cover plate. The head of the horizontal bracing rod is connected to the pressure cover plate via ball joints.

2.3 Friction force measurement

Friction between the bottom of the carriage and the guide rails, as well as between the steel laminations, can influence the accuracy of the test results. These frictions lead to a reduction in the actual shear stress applied to the specimen compared to the designed value. On one hand, this reduction causes a decrease in the measured strength parameters, while on the other hand, it underestimates the corresponding shear strain. Therefore, to establish the validity and reliability of the new direct simple shear apparatus, friction was experimentally measured.

The friction between the bottom of the carriage and the guide rails was tested following the procedure outlined below. Metal objects with different were placed on the carriage, and a horizontal servo motor pulled the carriage horizontally. The tension force F_1 exerted by the servo motor corresponding to different vertical pressures F_{N1} (including the weight of the metal objects, the carriage, and the steel laminations) was measured. Fig. 7 shows the test results. It can be seen that there is a strong linear fit between tension force F1 and the vertical pressure F_{N1}, with a fitting correlation coefficient of 0.986. The slope of the fitted line represents the friction coefficient between the bottom of the carriage and the guide rails, which is 0.027. The friction that is related to the vertical pressure applied the specimen cannot be ignored, even though it is very small. The calibration of the friction will be discussed in the next section combining with the experimental results.

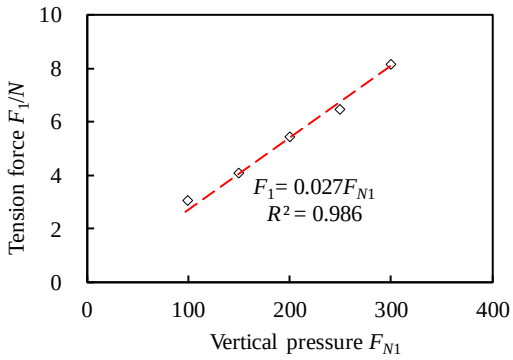

Fig. 7 Curve of frictional force for the bottom of the carriage and the rail

Furthermore, the frictions between the steel laminations were measured. The steel laminations were placed on the bottom plate of the carriage. Different vertical pressures F_{N2} were applied to the top layer of the steel laminations. The servo motor was used to horizontally slide the carriage. The corresponding tension force F_2 on the servo motor was measured. The frictions between the laminations were calculated by subtracting the friction F_1 between the bottom

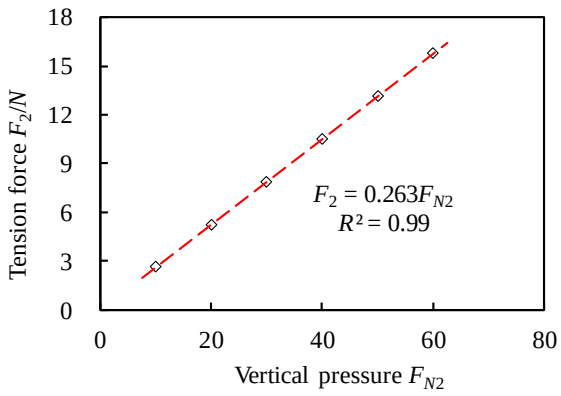

Fig. 8 Curve of frictions between the steel laminations

of the carriage and the guide rails from F_2. Fig. 8 shows the curve of frictions between the steel laminations. The calculated friction coefficient is 0.263.

In the experiment, the vertical pressure between the steel laminations is primarily due to the weight of the steel laminations. The total weight of all the steel laminations is only 5.48 N, the maximum friction between the steel laminations layers (on the top surface of lamination B) can be calculated as 1.44 N. The friction is relatively small in comparison to the shear force and can be ignored.

2.4 Technical advantages of the novel stress/strain-controlled direct simple shear apparatus

The novel direct simple shear apparatus offers several significant technical advantages:

(1) The outer frame for placing the steel laminations prevent soil particles from being squeezed between the layers of steel laminations during specimen preparation and consolidation. It effectively controls unidirectional sliding of the laminations along the horizontal shear direction.

(2) The aspect ratio of the internal dimensions of the steel laminations for specimen placement is 2.5:1. The design reduces the tendency for the specimen to tip and rotate after shearing deformation, leading to a more uniform distribution of shear stress along the surface of the specimen.

(3) The deformation control rods effectively ensure equal displacement difference between adjacent laminations. It facilitates uniform shear deformation of the soil.

(4) In shearing test, the friction between the steel laminations are minuscule compared to the shear force and can be ignored. The friction at the bottom of the carriage between the guild rail can be calibrated.

(5) The horizontal bracing rod provides support for the pressure cover plate, reducing the bending moment of loading rod and minimizing friction between the loading rod and the sleeve during shearing.

(6) The vertical force transmission structure adapts well to variations in the horizontal position of the loading rod pivot when subjected to vertical loading.

Table 1 Main physical-mechanical parameters of soils

Type of soils	ρ/(g/cm^3)	Gs	w/%	w_l/%	w_p/%	I_l	I_p
SSA	1.917	2.77	31.64	40.21	21.85	0.55	18.36
SSB	1.910	2.75	32.93	37.08	17.67	0.74	19.41

3. Preliminary test results and analysis

3.1 Test soil

To verify the performance of the novel apparatus, Using the novel apparatus, strain-controlled and stress-controlled experiments were conducted separately on two types of undisturbed soil, in-situ soil A (referred to as SSA) and in-situ soil B (referred to as SSB). Shear strength tests and creep tests were conducted on the soils. The main physical-mechanical parameters of soils are listed in Table 1. It can be observed that SSA and SSB belong to low liquid limit clay. According to consolidation test (not shown in this manuscript), the pre-consolidation pressure of the clay is 1900 kPa.

3.1 Shear strength test results and analysis

The novel apparatus was used to determine the shear strength parameters of SSA and SSB under saturated conditions by consolidation drained shear tests. The vertical pressures were set at 100, 200, 500, and 1000 kPa, with a consolidation time of 24 hours. The water in the sample is discharged through permeable plates located on both sides of the steel laminations. Due to a lack of criterion for testing the shear strength of soil using a direct simple shear apparatus, this paper refers to direct shear tests in ASTM D3080-03 (consolidation drained shear tests i.e. slow shear tests). A shear rate of 0.015 mm/min was applied. Shearing was stopped either when the shear stress reached its peak or when it plateaued. Fig. 9 shows the pictures of soil failure. It is observed that the failure surface is close to the horizontal plane. It can be found that there are no soil particles between adjacent steel laminates, and only water droplets seep out of the steel laminates during shearing.

Taking SSA as an example, Fig. 10 presents the relationship between shear stress τ and shear strain γ of the soil under different vertical pressures p. It can be observed that as the shear strain γ increases, the shear stress τ initially increases rapidly and then slows down until it reaches a stable value, which corresponds to the shear strength τ_f. As the vertical pressure p increases, the failure shear strain corresponding to the stable shear stress also increases. For instance, at a pressure of 100 kPa, the shear strength is 59.8 kPa, and the failure shear strain is 18.1%. At a pressure of 500 kPa, the shear strength increases to 297.1 kPa, with the failure shear strain reaching 34.15%. From the above results, it can be preliminarily concluded that the failure shear strain is related to the vertical pressure. The failure shear strain may reach larger values at higher vertical pressures. If the final failure shear strain of laboratory test is low, it may underestimate the strength of the soil.

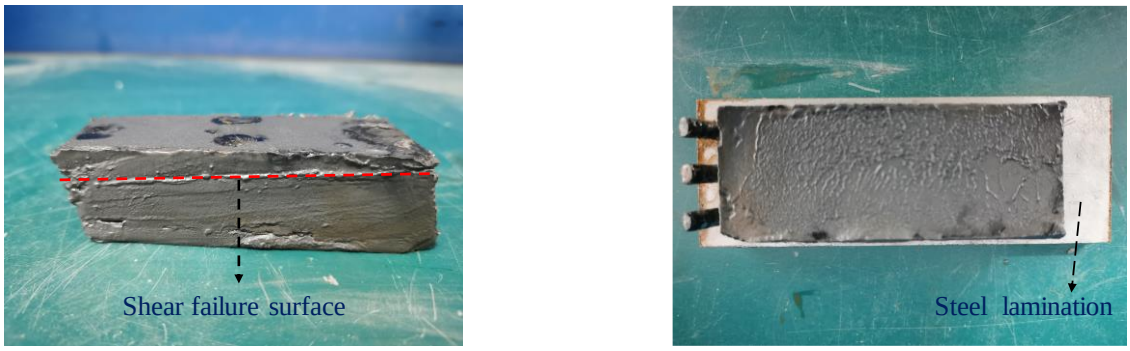

(a) (b)

Fig. 9 Pictures of soil shear failure

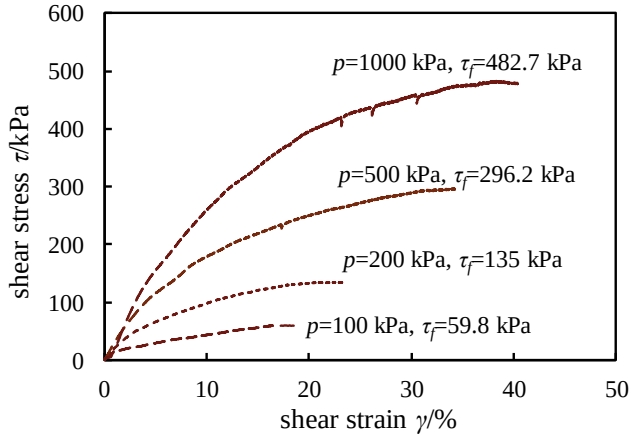

Fig. 10 Stress-strain curve of SSA under different vertical pressures

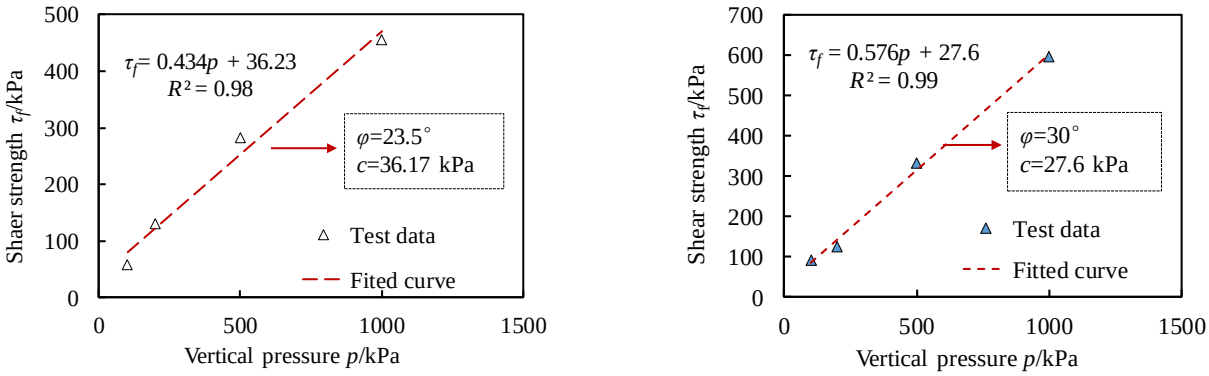

(a) Novel direct simple apparatus (b) Direct shear apparatus

Fig. 11 Shear strength under different vertical pressures of SSA

It is worth noted that, as described in section 2.3, the shear stress measured by the horizontal force sensor is affected by friction during shearing and should be calibrated. The shear force measured includes the force of soil resistance to shear and the friction force. Therefore, the shear strength of the soil under different vertical consolidation pressures is equal to the measured shear stress minus the friction.

The friction at the bottom of the carriage was studied based on the vertical pressures set in this section. The shear surface area of the sample is 40 cm^2. The normal force at the bottom of the carriage can be calculated based on the applied vertical pressures. The friction can be computed using the friction coefficient mentioned in section 2. The results are summarized in Table 2. Based on the measured shear strength at different vertical pressures, the shear force at the time of specimen failure can be obtained. The actual shear force applied to the specimen can be computed based on the corresponding friction, and thereby the shear strength of soil be calibrated.

Furthermore, Figs. 11 and 12 provide the shear strength of SSA and SSB under different vertical pressures. From

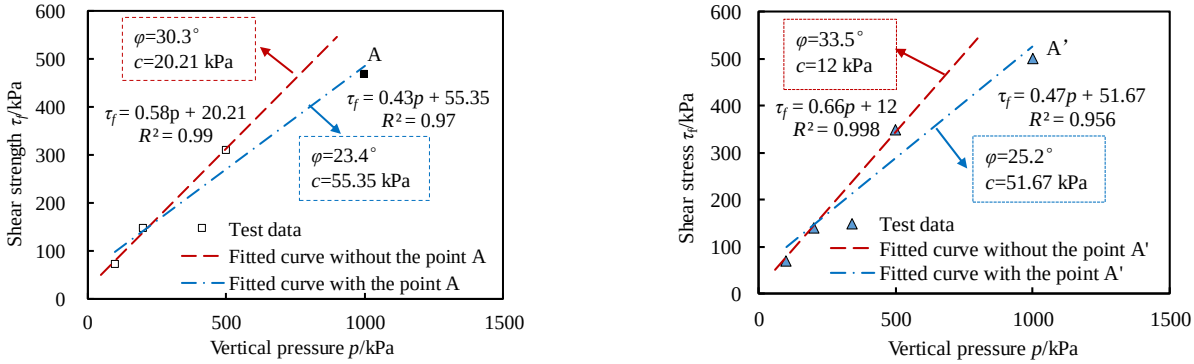

(a) Novel direct simple apparatus (b) Direct shear apparatus

Fig. 12 Shear strength under different vertical pressures of SSB

Fig. 11(a), it is evident that SSA exhibits a pronounced linear relationship between shear strength and vertical pressures, with a linear correlation coefficient of 0.98. The measured effective internal friction angle for SSA is 23.5°, and the effective cohesion is 36.23 kPa. Meanwhile, the shear strength of SSA is measured by a direct shear apparatus. The results are shows in Fig. 11(b). The effective internal friction angle of SSA measured by the direct shear apparatus is 30°, and the effective cohesion is 27.6 kPa. It is found that the effective internal friction angle measured by the novel direct simple shear apparatus is lower 6.5° than the direct shear apparatus, while the effective cohesion measured by the novel direct simple shear apparatus is higher 8.63 kPa than the direct shear apparatus. The reason for this difference is that the shear surface of the direct shear test is different from that of the direct simple shear test.

In Fig. 12, SSB displays different strength characteristics compared to SSA. At lower vertical pressures (below 500 kPa), there is a strong linear correlation between shear strength and vertical pressure, with a linear correlation coefficient of 0.99. Under the condition, SSB exhibits an effective internal friction angle of 30.3° and an effective cohesion of 20.21 kPa. However, at higher vertical pressures, specifically when the vertical pressure reaches 1000 kPa, the experimental values deviate from the fitted curve. The effective internal friction angle is 23.4° and the effective cohesion is 55.35 kPa if the result of p=1000 kPa is included. The shear strength of SSB at p=1000 kPa is lower than that derived from the linear regression, indicating significant non-linearity. The result is similar to the research of Dang *et al*. (2021).

Similarly, the shear strength of SSB is measured by a direct shear apparatus. The results are shows in Fig. 12(b). The linear effective internal friction angle of SSB measured by the direct shear apparatus is 33.5°, and the linear effective cohesion is 12 kPa. It is observed that the strength measured by the direct shear apparatus is slightly higher than that measured by the novel direct simple shear apparatus. This may be due to the fact that the failure surface of the direct shear test is not the weakest surface of the SSB.

The non-linear shear strength behavior of SSB may be attributed to the loose arrangement of clay particles at lower stress levels, where shear stress transmission primarily occurs through direct particle-to-particle contact. As stress levels increase, particles undergo reorganization and gradually compact, leading to structural changes within the soil. This structural change weakens the potential for strength development within the soil, resulting in non-linear growth of shear strength. A study by Wang *et al*. (1979) investigated the strength of clay under high pressure, revealing notable differences in the stress-strain relationship compared to low confining pressure conditions. This disparity is characterized by ductile yield, strain hardening, subsequent peak holding stages with a larger deformation range, as well as strength reduction with larger deformation. Consequently, for soils exhibiting non-linear strength characteristics like SSB, it is crucial to consider segmented strength profiles under different vertical pressures when utilizing shear strength parameters (Yazdani Bejarbaneh *et al*. 2015).

It is affirmed that the novel apparatus is not only capable of capturing the linear strength characteristics of soils but also able to describe their non-linear shear strength features. This validation shows the credibility and suitability of the developed apparatus for such studies.

3.2 Creep test results and analysis

Drained consolidation creep tests were conducted on the SSA and SSB using the developed apparatus. The vertical pressure for the tests was set at 100 kPa. After the consolidation of simple achieving stable, incremental shear stresses were applied corresponding to shear stress levels (defined as the ratio of shear stress τ to failure shear stress τ_f) of 0.2, 0.4, 0.6, and 0.8, respectively. Referring to the triaxial shear creep test of clay, the test stabilization time is generally around 7 days (Aktaa and Schinke 1996, Karunawardena *et al*. 2011, Wang *et al*. 2019, 2022). Therefore, in the work, the duration of each shear stress level was designed to be 5 to 10 days. However, the actual duration should be determined based on the creep stabilization of the soil. The next level of load was applied only after shear deformation was stabilized. There is currently no standardized creep stability standard for clay,

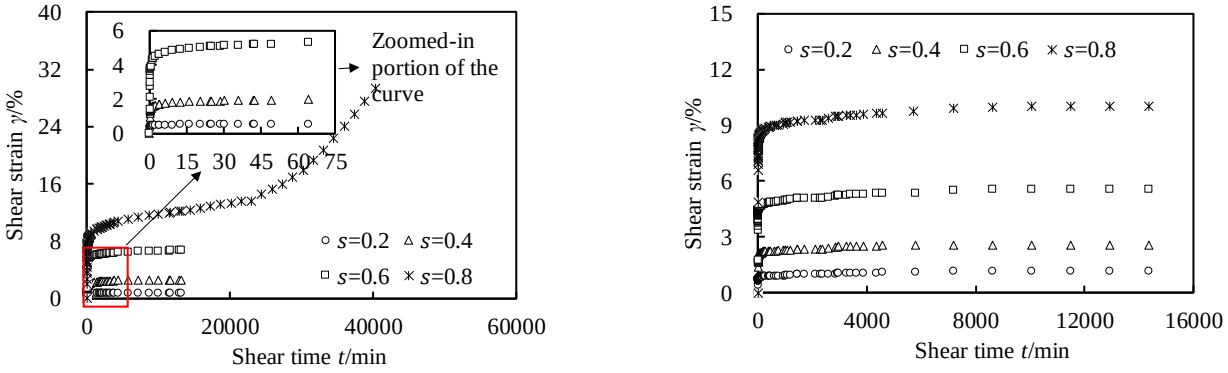

(a) SSA (b) SSB

Fig. 13 γ-t curve at vertical pressure of 100 kPa

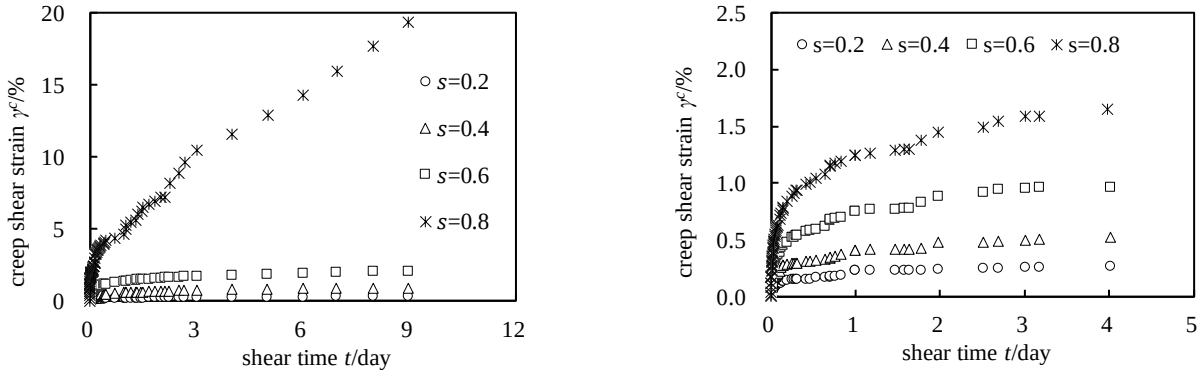

(a) SSA (b) SSB

Fig. 14 Creep curve at vertical pressure of 100 kPa

and it is generally believed that the deformation within 24 hours is less than 0.01mm to achieve creep stability. This approach ensures that the results of the staged loading test are more reliable and closer to those of a single loading test. Fig.13 depicts the creep curve γ-t.

From Fig. 13, it can be observed that at low stress levels (s=0.2, 0.4, 0.6), the shear strain-time behavior of both soils can be divided into two stages of the decaying and stable creep. In the early stages of creep, shear strain continues to increase but at a gradually decreasing rate. In the later stages, shear strain gradually stabilizes. At lower stress levels, the soils reach stability quickly. However, with increasing stress levels, the soils exhibit a significantly prolonged duration to reach creep stability, accompanied by a concurrent increase in the corresponding shear strain at the point of stabilization. For instance, at stress levels of s=0.2 and s=0.4, shear strain of SSB stabilizes by the 3rd day, with corresponding shear strains of 1.07% and 2.51%, respectively. However, at s=0.6, it requires a duration of 7 days to achieve stability, resulting in a shear strain of 10.02%.

At higher stress level (s=0.8), the creep test results for SSA and SSB exhibit different creep properties. Fig. 10a shows that the shear strain of SSA displays three creep stages of the decaying, stable and accelerating creep. Whereas Fig. 10b illustrates that SSB still exhibits decaying, stable creep at a shear stress level of 0.8. These test results demonstrate that the developed direct simple shear apparatus can describe various creep characteristics of soils, making it highly versatile and applicable.

It is worth noting that Fig. 13 shows the total shear strain curve. In the initial stage of loading, because the pore water was not expelled in time, the pore water pressure increased, causing the effective vertical stress to continuously decrease, resulting in significant shear deformation. After the pore water dissipated, the measured shear strain at this time is the creep shear strain, which is the post-construction shear deformation of concern, as shown in Fig. 14.

4. Discussion

Laboratory geotechnical tests aim to accurately simulate the behavior of the soil at a certain point in engineering. The direct simple shear test can achieve the aim only when stress and strain are uniform, which is often challenging to fully meet. The soil undergoes compressive deformation when subjected to vertical pressure. Even though Vaseline is applied to the inner walls of the steel laminations, the sidewall friction exerted on the soil by the inner walls of the steel laminations can only be reduced but not eliminated. Therefore, during the transmission of vertical pressure from top to bottom of specimen, the vertical force gradually

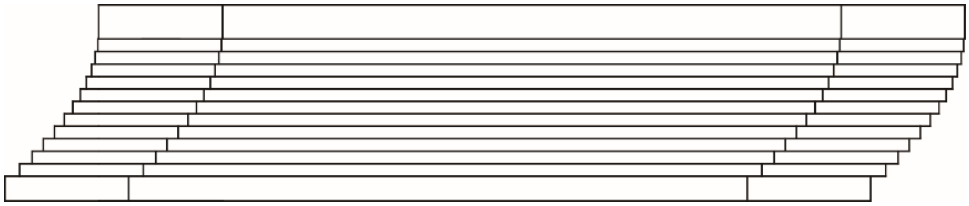

Fig. 14 Schematic diagram of unequal relative displacements between adjacent steel laminations

decreases due to the influence of sidewall friction on the steel laminations.

For example, assuming the vertical pressure applied by the lever is p, the thickness of each steel lamination is the same, and the sidewall friction force of the i-th layer (counting from the top) of steel laminations is f_{ci}. Then, the total vertical pressure F_i on the soil layer surrounded by the i-th steel lamination is calculated as

$$F_i = p - \sum_{i=1}^{i} f_{ci} \tag{1}$$

Thus, the vertical stress on the soil surrounded by the i-th shear layer can be calculated as

$$\sigma_i = F_i / A \tag{2}$$

where A is the cross-sectional area of the soil specimen. As i increases, σ_i decreases from top to bottom of specimen. Based on

$$\tau_{fi} = c + \sigma_i \tan\varphi \tag{3}$$

where c is cohesion of soil, φ is internal friction angle of soil. When c and φ remain constant, the vertical stress σ_i decreases from top to bottom of specimen, resulting in a gradual decrease in the shear strength τ_{fi} for each shear layer. Consequently, the shear strength distribution of the soil is non-uniform, with the strength decreasing towards the bottom. When a horizontal shear stress τ is applied to soil, exceeding its natural strength, it induces shear deformation, causing horizontal displacement of the steel laminations. Given that the applied horizontal shear stress remains uniform, while the soil strength decreases with depth, the lower steel laminations are more prone to sliding, leading to non-uniform soil shear deformations. Macroscopically, there are unequal relative displacements between adjacent layers of steel laminations, as depicted in Fig. 14. Therefore, it becomes a challenge to calculate shear strain across the entire plane of the soil.

To achieve a uniform shear deformation, a pin-type deformation control rod is introduced. It ensures equal relative displacements between adjacent steel laminations (Fig. 4). The effective height for shear is the total height formed by all the thin laminations. Since the shear strain for each steel lamination is

$$\gamma = \Delta x / 2 \tag{4}$$

where Δx is equal, the shear strain for each steel lamination is equal. This ensures a uniform shear strain distribution within the vertical plane perpendicular to the shear force.

Every apparatus encounters certain issues in its initial development stage, and the developed direct simple shear apparatus is no exception. Lamination B is dragged, causing displacement in the upper thin steel laminations. It is necessary to study whether the deformation control rod affects the strength of the soil. During the study, a comparison is needed between the stress and deformation of each steel lamination and the stress and deformation across the entire plane.

In addition, the extension of specimen ends during shearing results in the absence of complementary shear stresses at the ends, leading to nonuniform shear stress distribution across the specimen's top and bottom surfaces, with stress diminishing to zero at the corners (Boylan and Long 2009). This imbalance necessitates compensation through a nonuniform distribution of normal stress on the specimen's surfaces (Airey *et al*. 1985). However, the current direct simple apparatus only measures total vertical normal stress and total horizontal shear stress without providing insights into stress uniformity or the true stress state within the specimen. Hence, future improvements are imperative. Solutions proposed by Budhu (1979) and Airey (1984) serve as valuable groundwork for enhancing the apparatus to accurately assess stress uniformity and the true stress state during shearing.

5. Conclusions

A novel stress/strain-controlled direct simple shear apparatus has been developed and preliminary laboratory shear strength and creep tests have been conducted to demonstrate the effectiveness of the developed apparatus. The main findings are concluded as follows:

(1) The novel direct simple shear apparatus can prevent specimen overturning and stress concentration, achieve uniform shear of the specimen, and solve the problem of pivot displacement. This apparatus has a simple structure, low friction and high accuracy.

(2) The apparatus can capture both the linear and nonlinear strength properties of clay and exhibit notable applicability in predicting clay creep. Using this apparatus to determine the strength and deformation characteristics of soil is undoubtedly feasible.

(3) In direct simple shear strength test, significant failure shear strains may occur. Therefore, it is advisable not to set the maximum shear strain too low when conducting direct shear strength tests on soil. The tested soil exhibits pronounced creep characteristics. As the shear stress level increases, the creep duration and steady shear strain increase.

(4) Due to the fact that the vertical load of the novel developed apparatus is applied through a lever system, it is not possible to conduct consolidated undrained shear tests. Therefore, the apparatus will be further improved by adding a servo motor for applying vertical load.

Acknowledgments

This work was supported by the scientific project from Huaneng company Headquarters (HNKJ20-H45), Science and Technology Major Project of Tibetan Autonomous Region of China (XZ202201ZD0003G), Key Support Project of the Yangtze River Water Science Research Joint Fund (U2040221), the Natural Science Foundation of Jiangsu Province (No. BK20230954).

References

ASTM D3080-03, Standard test method for direct shear test of soils under consolidated drained conditions.

Airey, D.W. (1984), "Clays in circular simple shear apparatus", Ph.D. Dissertation, University of Cambridge, London.

Airey, D.W., Budhu, M. and Wood, D.M. (1985), "Some aspects of the behaviour of soils in simple shear", *Develop. Soil Mech. Found. Eng.*, 185-213. https://doi.org/10.1016/0148-9062(86)92342-9.

Airey, D.W. and Wood, D.M. (1987), "An evaluation of direct simple shear tests on clay", *Geotechnique*, **37**(1), 25-35. https://doi.org/10.1680/geot.1987.37.1.25.

Aktaa, J. and Schinke, B. (1996), "Creep lifetime under constant load and constant stress: theory and experiment", *J. Test Eval.*, **24**(4), 212-222. https://doi.org/10.1520/JTE11443J.

Anderson, S.A. and Riemer, M.F. (1995), "Collapse of saturated soil due to reduction in confinement", *J. Geotech. Eng.*, **121**(2), 216-220. https://doi.org/10.1061/(ASCE)0733-9410(1995)121:2(216).

Bjerrum, L. and Landva, A. (1966), "Direct simple-shear tests on a Norwegian quick clay", *Geotechnique*, **16**(1), 1-20. https://doi.org/10.1680/geot.1966.16.1.1.

Boylan, N. and Long, M. (2009), "Development of a direct simple shear apparatus for peat soils", *Geotech. Test. J.*, **32**(2), 126-138. https://doi.org/10.1520/GTJ101703.

Brandes, H.G. (2011), "Simple shear behavior of calcareous and quartz sands", *Geotech. Geol. Eng.*, **29**(1), 113-126. https://doi.org/10.1007/s10706-010-9357-x

Budhu, M. (1979), "Simple shear deformation of sands", Ph.D. Dissertation, University of Cambridge, London.

Budhu, M. (1984), "Nonuniformities imposed by simple shear apparatus", *Can. Geotech. J.*, **21**, 125-137. https://doi.org/10.1016/0148-9062(84)90401-7.

Budhu, M. and Britto, A.M. (1987), "Numerical analysis of soils in simple shear devices", *Soils Found.*, **27**(2), 33-46. https://doi.org/10.1016/0148-9062(88)91925-0.

Budhu, M. (1988), "Failure state of a sand in simple shear", *Can. Geotech. J.*, **25**(2), 395-400. https://doi.org/10.1139/t88-041.

Cappellaro, C., Cubrinovski, M., Bray, J.D., Chiaro, G., Riemer, M.F. and Stringer, M.E. (2021), "Liquefaction resistance of Christchurch sandy soils from direct simple shear tests", *Soil Dyn. Earthq. Eng.*, **141**, 106489. https://doi.org/10.1016/j.soildyn.2020.106489.

Chu, J., Leong, W.K., Loke, W.L. and Wanatowski, D. (2012), "Instability of loose sand under drained conditions", *J. Geotech. Geoenviron. Eng.*, **138**(2), 207-216. https://doi.org/10.1061/(ASCE)GT.1943-5606.0000574.

Dang, W., Konietzky, H., Herbst, M. and Thomas, F. (2017), "Complex analysis of shear box tests with explicit consideration of interaction between test device and sample", *Measurement*, **102**, 1-9. https://doi.org/10.1016/j.measurement.2017.01.040.

Dang, W., Chen, J., Huang, L., Ma, J. and Li, X. (2021), "Frictional behavior of granular materials exposed to dynamic normal load", *Eng. Geol.*, **295**, 0013-7952. https://doi.org/10.1016/j.enggeo.2021.106414.

DeGroot, D.J., Ladd, C.C. and Germaine, J.T. (1996), "Undrained multidirectional direct simple shear behavior of cohesive soil", *J. Geotech. Eng.*, **122**(2), 91-98. https://doi.org/10.1061/(ASCE)0733-9410(1996)122:2(91)

Doroudian, M. and Vucetic, M. (1995), "A direct simple shear device for measuring small-strain behavior", *Geotech. Test. J.*, **18**(1), 69-85. https://doi.org/10.1520/GTJ10123J.

Hubler, J.F., Athanasopoulos-Zekkos, A. and Zekkos, D. (2017), "Monotonic, cyclic, and postcyclic simple shear response of three uniform gravels in constant volume conditions", *J. Geotech. Geoenviron. Eng.*, **143**(9), 04017043. https://doi.org/10.1061/(ASCE)GT.1943-5606.0001723.

Jin, H., Guo, L., Sun, H., Shi, L. and Cai, Y. (2022), "Undrained cyclic shear strength and stiffness degradation of overconsolidated soft marine clay in simple shear tests", *Ocean Eng.*, **262**, 112270. https://doi.org/10.1016/j.oceaneng.2022.112270.

Jurko, J., Sassa, K. and Fukuoka, H. (2008), "Study on seismic behavior of nonplastic silt by means of ring-shear apparatus". Landslides, 5, 189–201. https://doi.org/10.1007/s10346-008-0113-8

Karunawardena, A., Oka, F. and Kimoto, S. (2011), "Elasto-viscoplastic modeling of the consolidation of Sri Lankan peaty clay", *Geomech. Eng.*, **3**(3), 233-254. http://dx.doi.org/10.12989/gae.2011.3.3.233.

Khayat, N., Ghalandarzadeh, A. and Jafari, M.K. (2014), "Grain shape effect on the anisotropic behavior of silt-sand mixtures", *Geotech. Eng.*, **167**(3): 281-296. http://dx.doi.org/10.1680/geng.11.00093.

Khayat, N. (2018), "Monotonic behaviour of sand under torsional loading with different confine stress", *Int. J. Geomate*, **14**(43), 148-153. https://doi.org/10.21660/2018.43.7359.

Kjellman, W. (1951), "Testing the shear strength of clay in Sweden", *Geotechnique*, **2**(3), 225-232. https://doi.org/10.1680/geot.1951.2.3.225.

Kwan, S.W. (2018), "A review on sand specimen reconstitution methods and procedures for undrained simple shear test", *Int. J. Geotech. Eng.*, 1-9. https://doi.org/10.1080/19386362.2018.1461988.

Lashkari, A., Falsafizadeh, S.R., Shourijeh, P.T. and Alipour, M.J. (2020), "Instability of loose sand in constant volume direct simple shear tests in relation to particle shape", *Acta Geotechnica*, **15**(9), 2507-2527. https://doi.org/10.1007/s11440-019-00909-4.

Lashkari, A., Falsafizadeh, S.R. and Rahman, M.M. (2021), "Influence of linear coupling between volumetric and shear strains on instability and post-peak softening of sand in direct simple shear tests", *Acta Geotechnica*, **16**(11), 3467-3488. https://doi.org/10.1007/s11440-021-01288-5.

Li, Y., Yang, Y., Yu, H.S. and Roberts, G. (2017), "Monotonic direct simple shear tests on sand under multidirectional loading", *Int. J. Geomech.*, **17**(1), 04016038. https://doi.org/10.1061/(ASCE)GM.1943-5622.0000673.

Mayne, P.W. (1985), "A review of undrained strength in direct simple shear", *Soils Found.*, **25**(3), 64-72. https://doi.org/10.3208/sandf1972.25.3_64.

Medicus, G., Kwa, K.A. and Cerfontaine, B. (2022), "A consistent calibration process for the Matsuoka–Nakai friction angle under direct simple shear conditions for clay hypoplasticity", *Comput. Geotech.*, **150**, 104888. https://doi.org/10.1016/j.compgeo.2022.104888.

Muhammad, N.N., Seung, H.L., Song, H.C. and Jae, H.K. (2023), "Modification of direct shear apparatus for soil-soil and soil-solid interface testing", *Geomech. Eng.*, **35**(3), 325-332. https://doi.org/10.12989/gae.2023.35.3.325.

Monkul, M.M., Gültekin, C., Gülver, M., Akın, Ö. and Eseller-Bayat, E. (2015), "Estimation of liquefaction potential from dry and saturated sandy soils under drained constant volume cyclic simple shear loading", *Soil Dyn. Earthq. Eng.*, **75**, 27-36. https://doi.org/10.1016/j.soildyn.2015.03.019.

Mortezaie, A. and Vucetic, M. (2012), "Small-strain cyclic testing with standard NGI simple shear device", *Geotech. Test. J.*, **35**(6), 935-948. https://doi:10.1520/GTJ20120007.

Mortezaie, A.R. and Vucetic, M. (2013), "Effect of frequency and vertical stress on cyclic degradation and pore water pressure in clay in the NGI simple shear device", *J. Geotech. Geoenviron. Eng.*, **139**(10), 1727-1737. https://doi.org/10.1061/(ASCE)GT.1943-5606.0000922.

Nong, Z.Z., Park, S.S. and Lee, D.E. (2021), "Comparison of sand liquefaction in cyclic triaxial and simple shear tests", *Soils Found.*, **61**(4), 1071-1085. https://doi.org/10.1016/j.sandf.2021.05.002.

Rasool, A.M. and Aziz, M. (2019), "Shear infiltration and constant water content tests on unsaturated soils", *Geomech. Eng.*, **19**(5), 435-445. https://doi.org/10.12989/gae.2019.19.3.269.

Reid, D. and Fourie, A. (2019), "A direct simple shear device to study static liquefaction triggering under constant shear drained loading", *Géotechnique Lett.*, **9**(2), 1-18. https://doi.org/10.1680/jgele.19.00011.

Reardon, R., Humire, F., Ahmed, S.S., Ziotopoulou, K., Martinez, A. and DeJong, J.T. (2022), "Effect of gradation on the strength and stress-dilatancy of coarse-grained soils: a comparison of monotonic direct simple shear and triaxial tests", *Proceedings of the Geo-Congress*, 226-236. https://doi.org/10.1061/9780784484678.031.

Roscoe, K.H. (1953), "An apparatus for the application of simple shear to soil samples", *Proceedings of the 3rd International Conference on Soil Mechanics and Foundation Engineering*, Zurich.

Tao, K., Dang, W. and Li, Y. (2023), "Frictional sliding of infilled planar granite fracture under oscillating normal stress", *Int. J. Min. Sci. Tech.*, **33**(6), 687-701. https://doi.org/10.1016/j.ijmst.2022.12.001.

Vieira, C.S., Lopes, M.D. and Caldeira, L. (2015), "Sand-nonwoven geotextile interfaces shear strength by direct shear and simple shear tests", Geomech. Eng., **9**(5), 601-618. https://doi.org/10.12989/gae.2015.9.5.601.

Vucetic, M. and Lacasse, S. (1982), "Specimen size effect in simple shear test", *J. Geotech. Eng. Division*, **108**(12), 1567-1585. https://doi.org/10.1061/AJGEB6.0001395.

Vucetic, M., Lanzo, G. and Doroudian, M. (1998), "Effect of the shape of cyclic loading on damping ratio at small strains", *Soils Found.*, **38**(1), 111-120. https://doi.org/10.3208/sandf.38.111.

Wai, D., Manmatharajan, M.V. and Ghafghazi, M. (2022), "Effects of imperfect simple shear test boundary conditions on monotonic and cyclic measurements in sand", *J. Geotech. Geoenviron. Eng.*, **148**(1), 04021164. https://doi.org/10.1061/(ASCE)GT.1943-5606.0002682.

Wahyudi, S., Koseki, J., Sato, T. and Chiaro, G. (2016), "Multiple-liquefaction behavior of sand in cyclic simple stacked-ring shear tests", *Int. J. Geomech.*, **16**(5), C4015001. https://doi.org/10.1061/(ASCE)GM.1943-5622.0000596.

Wang, C.Y., Mao, N.H. and Wu, F. (1979), "The mechanical property of montmorillonite clay at high pressure and implications on fault behavior", *Geophys. Res. Lett.*, **6**(6), 476-478. https://doi.org/10.1016/0148-9062(80)91123-7.

Wang, C.Y. and Mao, N.H. (1979), "Shearing of saturated clays in rock joints at high confining pressures", *Geophys. Res. Lett.*, **6**(11), 825-828. https://doi.org/10.1029/gl006i011p00825.

Wang, T., Liu, S.H. and Lu, Y. (2019), "Laboratory experiments on the improvement of rockfill materials with composite grout", *Geomech. Eng.*, **17**(3), 309-318. https://doi.org/10.12989/gae.2019.17.3.307.

Wang, T., Liu, S.H., Wautier, A. and Nicot, F. (2022), "Updated skeleton void ratio for gravelly sand mixtures considering the effect of grain size distribution", *Can. Geotech. J.*, **59**(1), 12-23. https://doi.org/10.1139/cgj-2020-0570

Xu, D.S., Liu, H.B., Rui, R. and Gao, Y. (2019), "Cyclic and postcyclic simple shear behavior of binary sand-gravel mixtures with various gravel contents", *Soil Dyn. Earthq. Eng.*, **123**, 230-241. https://doi.org/10.1016/j.soildyn.2019.04.030.

Yazdani Bejarbaneh, B., Jahed Armaghani, D. and Mohd Amin, M.F. (2015), "Strength characterisation of shale using mohr–coulomb and hoek–brown criteria", *Measurement*, **63**(63), 269-281. https://doi.org/10.1016/j.measurement.2014.12.029.

Zhang, M., Yang, Y., Zhang, H. and Yu, H.S. (2019), "DEM and experimental study of bi-directional simple shear", *Granular Matter*, **21**, 1-13. https://doi.org/10.1007/s10035-019-0870-1.

Zhang, C., Ji, J., Gui, Y., Kodikara, J., Yang, S.Q. and He, L. (2016), "Evaluation of soil-concrete interface shear strength based on LS-SVM", *Geomech. Eng.*, **11**(3), 361-372. https://doi.org/10.12989/gae.2016.11.3.361.

GC